RSC Advances

PAPER

View Article Online
View Journal | View Issue

Cite this: *RSC Adv.*, 2021, **11**, 2656

pH and redox dual-sensitive drug delivery system constructed based on fluorescent carbon dots†

Boye Zhang,[a] Qianqian Duan,*[a] Yi Li,[b] Jianming Wang,[c] Wendong Zhang[a] and Shengbo Sang *[a]

Received 27th October 2020
Accepted 4th January 2021

DOI: 10.1039/d0ra09164b

rsc.li/rsc-advances

Herein, a pH and redox dual-responsive drug delivery system (CDs–Pt(IV)–PEG) was developed based on fluorescence carbon dots (CDs). In this system, cisplatin(IV) prodrug (Pt(IV)) was selected as a model drug to reduce toxic side effects. The aldehyde-functionalized monomethoxy polyethylene glycol (mPEG-CHO) was conjugated to CDs–Pt(IV) to form pH sensitive benzoic imine bond. Owing to the slightly acidic tumor extracellular microenvironment (pH 6.8), the benzoic imine bond was then hydrolyzed, leading to charge reversal and decrease in the hydration radius of the drug-carrying, which facilitated *in vivo* circulation and tumor targeting. Notably, the cytotoxicity of the drug delivery system on cancer cells was comparable to that of cisplatin, while the side effects on normal cells were significantly reduced. In addition, the system realized recognition of cancer cells by the high-contrast fluorescent imaging. In conclusion, the CDs–Pt(IV)–PEG system provided a promising potential for effective delivery of anticancer drugs and cancer cells screening.

Introduction

Cancer has become an emerging health issue in the world.[1–4] Recently, imaging-guided stimuli-responsive nanoscale drug delivery system for cancer therapy has attracted considerable attention and become one of the research hotspots in targeted cancer therapy.[5–9] In general, ideal multifunctional drug delivery system for targeted therapy of cancer through intravenous administration will firstly circulate in the blood, then accumulate at tumor sites and finally release the drugs after internalization into cancer cells.[10–12] However, it is required to overcome multiple obstacles for realizing these complex steps, because the specific requirements on charge, size or stability of nanocarrier at each stage are different.[13–16] Therefore, how to incorporate multiple nano-characteristics required at each stage into one nanocarrier system for overcoming multi-stage biological barriers remains a challenge.

Fluorescent carbon dots (CDs), as a novel type of fluorescent nanomaterials, have many advantages such as adjustable emission, good photostability, small size, and good biocompatibility.[17–20] Therefore, CDs exhibited broad biological applications and have been regarded as a preferred carrier for drug delivery systems.[21–24] In addition, polymer conjugates can be used to structure the coating layer of the drug delivery system, which can preferentially enter the cancer tissue *via* the enhanced permeability and retention (EPR) effect.[25,26] Furthermore, the carrier polymer can degrade *in vivo* and then effectively release the encapsulated cancer drugs under the cellular microenvironment.[27–30]

Here, a multi-strategy drug delivery system which integrated multiple nano-features into one nanoplatform was proposed, as shown in Scheme 1. Microenvironment-driven cascaded responsive drug delivery and CDs-based imaging tracking could be achieved simultaneously in this drug delivery system. At pH 6.8, the pH sensitive benzoic imine bond of CDs–Pt(IV)–PEG got hydrolyzed, resulting in the surface charge reversal and size decrease. Furthermore, after internalization, the cisplatin(IV) prodrug loaded in CDs–Pt(IV)–PEG was reduced to cisplatin in reductive cytosol of cancer cells, which showing significant cytotoxicity. This proposed CDs-based drug delivery system can improve the utilization efficiency of drugs and reduce the side effects in normal physiological condition.

Experimental section

Materials and apparatus

Citric acid, ammonia, cisplatin, 4-formylbenzoic acid, succinic anhydride, aldehyde-functionalized monomethoxy polyethylene glycol (mPEG-CHO) (2000 Da), 1-(3-dimethylaminopropyl)-3-ethylcarbodiimide hydrochloride (EDC·HCl), diethyl ether, acetone, dimethyl sulfoxide (DMSO),

[a]*MicroNano System Research Center, College of Information and Computer, Key Laboratory of Advanced Transducers and Intelligent Control System of the Ministry of Education and Shanxi Province, Taiyuan University of Technology, Taiyuan 030024, China. E-mail: wwhwls@163.com; sunboa-sang@tyut.edu.cn*

[b]*Theranostic Macromolecules Research Center, School of Chemical Engineering, Sungkyunkwan University, Suwon 16419, Republic of Korea*

[c]*Wound Repair Department, General Hospital of TISCO, Taiyuan 030003, China*

† Electronic supplementary information (ESI) available. See DOI: 10.1039/d0ra09164b

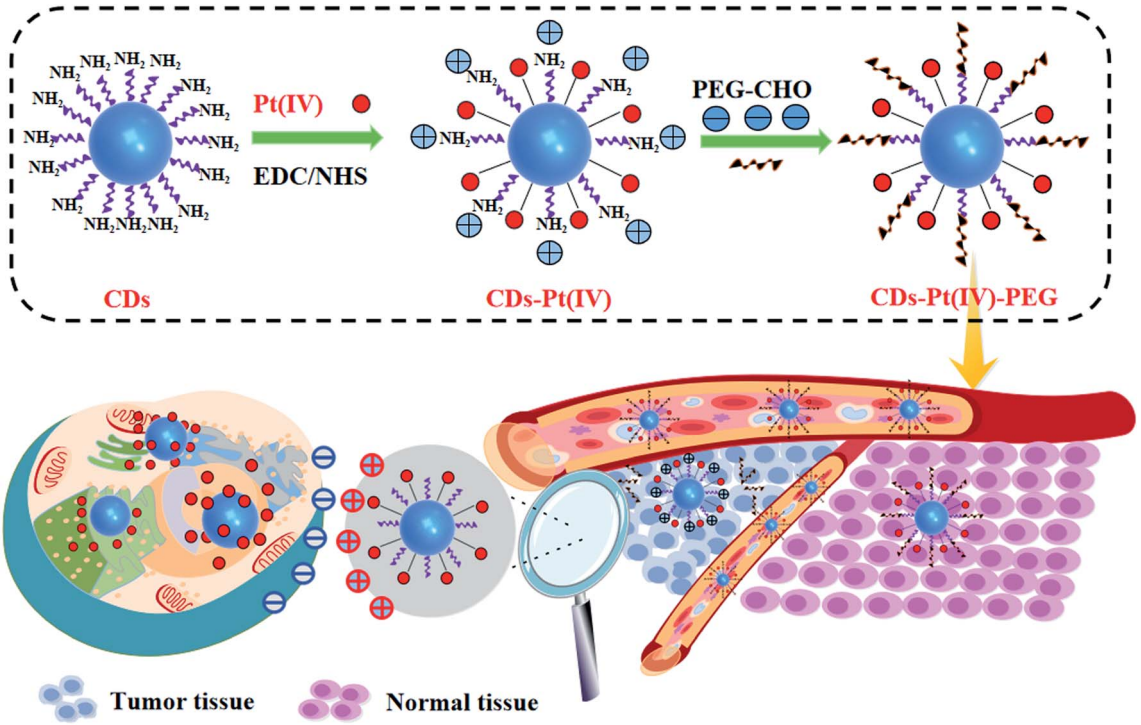

Scheme 1 Schematic diagram of CDs–Pt(IV)–PEG nano-delivery system.

hydrogen peroxide (30 wt%) and *N*-hydroxysuccinimide (NHS) were purchased from Sinopharm Chemical Reagent Company (Beijing, China). Human gastric cancer MGC-803 cells and normal gastric cell line GES-1 were provided by the Cell Bank of the Chinese Academy of Sciences (Shanghai, China). Dulbecco's Modified Eagle's Medium (DMEM) (pH 7.4 or 6.8), fetal bovine serum (FBS), and other reagents used for cell culture were purchased from Sangon Biotech (Shanghai, China). 3-[4,5-Dimethyl-2-thiazolyl]-2,5-diphenyl-2-tetrazolium bromide (MTT) were bought from Sigma (Missouri, USA). All reagents were of analytical grade and used without further purification. Ultrapure water purified by a Millipore Milli-Q system was used throughout the experiments.

The morphological characteristics of CDs were measured by a high-resolution TEM (JEOL-2100F, Tokyo, Japan). The surface functional groups of samples were performed using a Fourier transform infrared (FTIR) spectroscopy (Bruker Optik GmbH Tensor 27, Ettlingen, Germany). The absorption spectra were obtained from a UV-Vis spectrophotometer in the wavelength range 190–1200 nm (METASH UV-8000, Shanghai, China). Fluorescence spectra were evaluated using a FLS-980 fluorescence spectrophotometer (Edinburgh Instruments, Britain). The optical density (OD) values of MTT assay for cytotoxicity test were measured using a microplate reader (Multiskan Go, Thermo Scientific, USA). All images of cells were observed by fluorescence microscope (Leica DM3000, Wetzlar, Germany). Zeta potential and particle size of this system were measured using dynamic light scattering (DLS) (Malvern ZS90, Britain). Platinum loading percentage was determined by an Agilent 7800 inductively coupled plasma mass spectrometer (ICP-MS).

Preparation of CDs

CDs were synthesised from citric acid and ammonia by one-step hydrothermal method. Firstly, 2.1 g citric acid was dissolved in 20 mL ultrapure water to form a clear solution. Subsequently, add 2.25 mL ammonia water to the solution and continue to stir until completely dissolved. The mixture was then transferred into a 50 mL Teflon lined autoclave and heated at 180 °C for 10 h in a muffle furnace. After the reaction, the CDs solution was filtered through a 0.22 μm membrane and then dialyzed using a dialysis bag with molecular weight cut off (MWCO) of 1000 Da. Lastly, the resulting solution was frozen and lyophilized until green solid powder was attained.

Preparation of cisplatin(IV) prodrug

600.0 mg cisplatin was dissolved in 15 mL water, and followed by dropwise addition of 21 mL hydrogen peroxide (30 wt%) at 50 °C. The mixture solution was stirred for 2 h, cooled to room temperature, and then kept at 0 °C overnight. Finally, the resulting pale yellow solid that formed was collected by filtration, washed thoroughly with cold water and diethyl ether, and then dried *in vacuo*.[31]

Subsequently, the above product (40.0 mg) and succinic anhydride (120.0 mg) were completely dissolved in 16 mL DMSO. Then the mixed solution was stirred for 4 h at room temperature and freeze-dried. Lastly, the resulting solid was washed thoroughly with cold acetone and diethyl ether to obtain cisplatin(IV) prodrug (Pt(IV)).

Preparation of CDs–Pt(IV)

Briefly, 11 mg Pt(IV), 5.4 mg EDC·HCl and 3.7 mg NHS were dissolved in water, and stirred at room temperature for 1 h. Then 33 mg CDs were added to the above solution and stirred for 24 h. The mixed solution was dialysed against ultrapure water for 48 h to remove all unreacted compounds. After dialysis and lyophilization, CDs loaded with Pt(IV) (CDs–Pt(IV)) were stored at room temperature for further use.[4] The platinum loading of the obtained CDs–Pt(IV) measured by ICP-MS was 5.72 wt%.

Preparation of CDs–Pt(IV)–PEG

The obtained CDs–Pt(IV) and mPEG-CHO (4 mg) were dissolved in DMSO (1 mL) and stirred at 40 °C for 24 h under dark condition. Then the mixture solution was dialysed against water (pH 8, adjusted with NaOH) by dialysis membrane (MWCO 3.5 kDa) for 24 h to remove impurities. The dialysis membrane content was lyophilized and then the resulting CDs–Pt(IV)–PEG stored at −20 °C.

Cytotoxicity and cell imaging

MGC-803 and GES-1 cells were cultured with DMEM with 10% FBS in an air-5% CO_2 incubator at 37 °C.

Cell viability was determined by the MTT method. Briefly, cells were seeded in 96-well plates with an initial density of 1×10^4 per well. After the cells reached 80% confluency, the culture media was replaced by fresh media (at pH 6.8 or 7.4 with or without 1 mM GSH) containing CDs, cisplatin, or CDs–Pt(IV)–PEG for 24 h and 48 h, respectively. Cells without the treatment of CDs, cisplatin, or CDs–Pt(IV)–PEG were regarded as control group in every protocol. After incubation, 10 μL of MTT solution was then added to each well, and incubated at 37 °C for a further 4 h. Thereafter, the medium was discarded and followed by the addition of 100 μL of DMSO to each well to dissolve the violet formazan crystals. Lastly, the absorbance of each well was read immediately at 450 nm using a microplate reader.

MGC-803 (or GES-1) cells were seeded on glass slides in 24-well plates. After the cells reached 80% confluency, cells were then treated with one of the following protocols: (1) for GES-1 cells, the culture media was replaced with DMEM medium with pH 7.4 and treated with the prepared solution of CDs–Pt(IV)–PEG for 6 h; (2) for MGC-803 cells, the culture media was replaced with DMEM medium with pH 6.8 or 7.4 and treated with the prepared solution of CDs–Pt(IV)–PEG for 6 h, respectively. After incubation, cells were washed by PBS for three times and fixed with PBS containing 4% paraformaldehyde. And then the cells were observed under fluorescence microscopy with different excitation wavelengths (365, 488 and 543 nm). Finally, the fluorescence intensity was calculated by Image-Pro Plus 5.1.

Results and discussion

Characterization of the prepared materials

As shown in Fig. S1a,† in order to develop drug-loaded nanocarrier CDs–Pt(IV)–PEG, Pt(IV) was firstly synthesized based on cisplatin. Then Pt(IV) coupled with the CDs *via* the amidation reaction of EDC/NHS between the carboxylic acid group at Pt(IV) and some amino groups on CDs. To further fabricate a pH-responsive pharmaceutical nanocarrier, the mPEG-CHO was loaded over the other amino groups on CDs through benzoic imine bond formation.

The synthesized CDs had a uniform dispersion with an average size of 3.64 nm as judged from image analysis of 100 individual particles (Fig. 1a and S3†). According to the FTIR spectra (Fig. 1b), the broad vibration bands around 3000–3500 cm^{-1} corresponded to the stretching vibration of O–H and N–H. Moreover, bending vibration of N–H (1572 cm^{-1}) and stretching vibration of C–N (1325 cm^{-1}) were also observed, respectively, indicating that the surface of CDs was rich in amino groups. In addition, the ratio of the relative vibration intensities of C=O and N–H increased after loading the Pt(IV) on CDs. The strong absorption peak at 1047 cm^{-1} corresponded to the stretching vibration of C–O on PEG, demonstrating the successful functionalization of mPEG-CHO polymer.[5,6]

In order to further analyze the chemical features, UV-Vis absorption spectra were recorded. As can be seen in Fig. 1c, CDs displayed two absorption peaks at 234 nm and 334 nm, which belonged to the typical π–π* transition of C=C group and n → π* transition of C=O group, respectively. After loading Pt(IV) and PEG, the peak at 234 nm showed a slight blue shift and the intensity ratio of 234 nm/334 nm increased obviously, which may result from the changes in surface functional groups and size after the reaction of amide and aldimine condensation. The prepared CDs exhibited bright blue fluorescence, and the emission peak hardly changed with varying the excitation wavelength (Fig. 1d). The fluorescence intensity reached the maximum at the excitation wavelength of 360 nm. The fluorescence of the CDs resulted from the surface state trapping the energy of the excited state. Notably, the fluorescence spectra of CDs–Pt(IV)–PEG system (Fig. S2†) were similar to that of CDs. The effect of pH (pH = 1–14) on the fluorescence intensity of CDs was studied. The results showed that the fluorescence intensity of CDs was relatively stable except under extreme acidic and alkaline pH conditions (Fig. S4†). Especially, the fluorescence intensity exhibited excellent stability in the pH range of 4–12 (Fig. S4b†), which almost covering all the pH values of biological environment. Furthermore, the emission peak position of CDs hardly changed under the fixed excitation wavelength (Fig. S4a†). The results showed that the CDs have a very favorable fluorescence stability in a wide range of pH in terms of excitation/emission wavelengths and fluorescence intensity, which provides a logical basis for subsequent research on bioimaging and drug delivery.

In vitro cytotoxicity assay

An effective drug delivery system should be able to enhance the therapeutic effectiveness of cancer treatment while reducing side effects and/or avoiding. Considering the safety of the potential biomedical applications, the cytotoxicity of CDs, cisplatin, or CDs–Pt(IV)–PEG was evaluated by the MTT assays (Fig. 2). The MGC-803 and GES-1 cell lines were used as models. After either a 24 or 48 h incubation, the CDs displayed limited

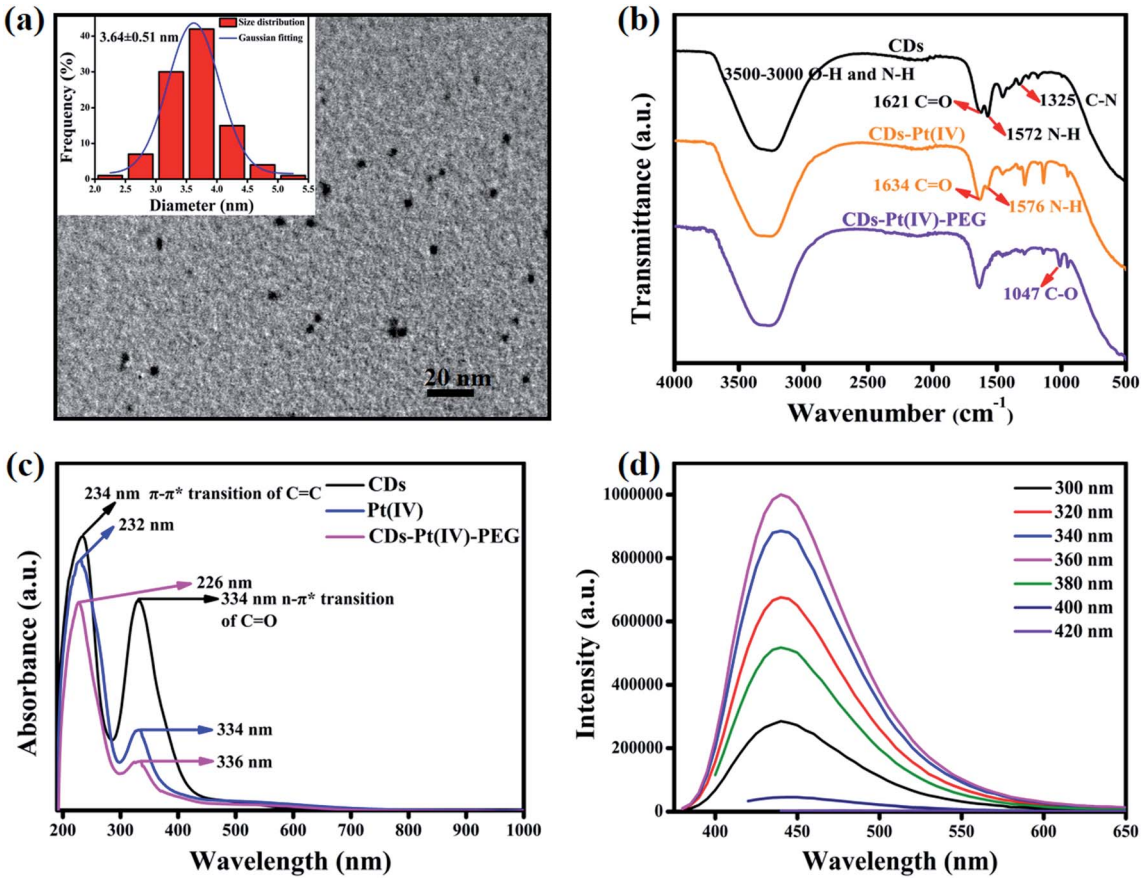

Fig. 1 (a) TEM image of CDs (inset: particle size distribution of CDs). (b) FTIR spectra of CDs, CDs–Pt(IV), and CDs–Pt(IV)–PEG. (c) UV absorption spectra of CDs, Pt(IV), and CDs–Pt(IV)–PEG. (d) Fluorescence spectra of CDs under different excitation wavelengths.

effect on cell viability in both cell lines with a viability of above 88% at all studied doses, indicating that the prepared CDs exhibit good biocompatibility. Thus the prepared CDs can be used as a fluorescence probe for cell imaging and drug delivery tracking. As shown in Fig. 2a and b, for human gastric cancer MGC-803 cells, the cytotoxicity of both CDs–Pt(IV)–PEG and cisplatin exhibited a dose- and time-dependent. Specifically, the cell viability rates were about 43.5% and 36.9% (CDs–Pt(IV)–PEG), 41.8% and 37.5% (cisplatin) after incubation at a concentration of 87 μg mL^{-1} for 24 h and 48 h, respectively. In addition, the cytotoxicity of CDs–Pt(IV)–PEG was almost equal to that of cisplatin after 24 h or 48 h incubation at the same concentration. As shown in Fig. 2c and d, for normal GES-1 cells, the cytotoxicity of CDs–Pt(IV)–PEG was obviously lower than that of cisplatin. Specifically, the cell viability rates were about 53.9% and 49.8% after incubation of CDs–Pt(IV)–PEG at a high concentration of 87 μg mL^{-1} for 24 h and 48 h, respectively, while only about 37.5% and 36.5% after incubation of cisplatin under the same conditions. These results showed that the developed CDs–Pt(IV)–PEG system exerted a tumor suppressive effect on cancer cells, and reduced side effects to normal cells.

To explore the pH-responsive behavior of the CDs–Pt(IV)–PEG system, the cancer MGC-803 cells were treated with CDs–Pt(IV)–PEG at pH 7.4 or pH 6.8 (Fig. 3). The CDs–Pt(IV)–PEG system exhibited a more obvious inhibition effect at pH 6.8 than pH 7.4, even for the same cell line. Additionally, to further evaluate the redox-sensitivity of CDs–Pt(IV)–PEG in the intracellular microenvironment. MGC-803 cells were pretreated with or without GSH (1 mM, a similar concentration inside cancer cells)[32] for simulating intracellular reductive microenvironment. Significant impairment of the cell viability was observed in the presence of GSH as compared with in the absence of GSH under the same pH value. The controlled release of cisplatin from CDs–Pt(IV)–PEG was confirmed under reducing conditions. These results were further proved the dual pH/reducing-responsive property.

IC_{50}, the half-maximal inhibitory concentration, represents the concentration of a compound that is required for 50% inhibition of things like a cell, a cell receptor or a microorganism. This quantitative measure indicates how much of a compound is needed to inhibit a given biological process by half.[33] To further provide the quantization parameter for the clinical application, the IC_{50} values were computed. As shown in Fig. S5,† the CDs–Pt(IV)–PEG system exhibited the IC_{50} values of 41.41 μg mL^{-1}, 25.41 μg mL^{-1}, 19.11 μg mL^{-1} and 16.86 μg mL^{-1} toward MGC-803 cells at pH 7.4, pH 6.8, pH 7.4 with GSH and pH 6.8 with GSH for 24 h, respectively. Similarly, the

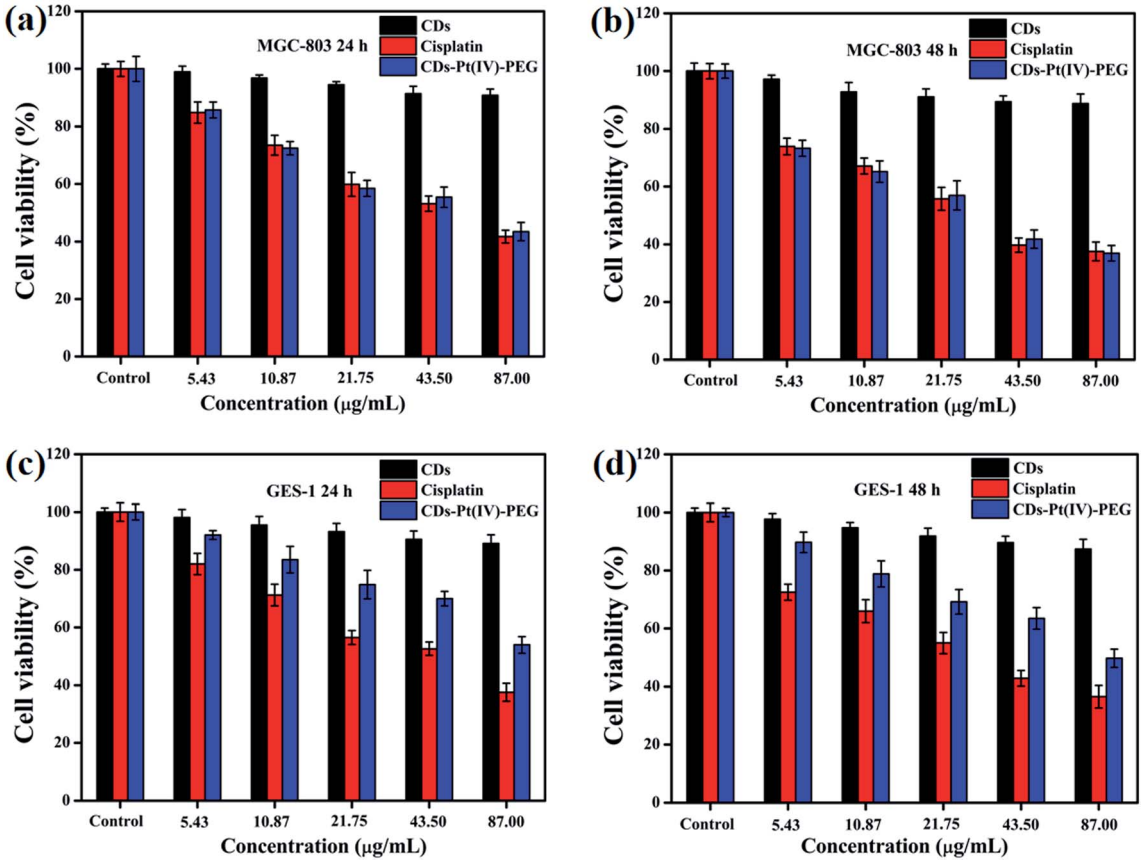

Fig. 2 Cell viability of (a and b) MGC-803 and (c and d) GES-1 cells after incubation of CDs, cisplatin, or CDs–Pt(IV)–PEG with different concentration for 24 h and 48 h, respectively.

corresponding IC_{50} values for 48 h were 20.60 μg mL^{-1}, 13.54 μg mL^{-1}, 11.17 μg mL^{-1} and 9.95 μg mL^{-1}, respectively. Thus, the pH- and redox-responsive controlled release under the intracellular microenvironment of cancer cells make the CDs–Pt(IV)–PEG a promising drug delivery system.

This may be due to the selective release of CDs–Pt(IV)–PEG controlled by the tumor microenvironment. As we all know, the benzoic imine bond is extremely sensitive to acidic condition, which might be hydrolyzed under pH 6.8 and not completely hydrolyzed under pH 7.4.

Cell imaging with CDs–Pt(IV)–PEG

For further studying the targeting ability of the developed drug nanocarrier system induced by the acidic tumor microenvironment and evaluating the cellular uptake capability of CDs–Pt(IV)–PEG, we performed comparative experiments on the

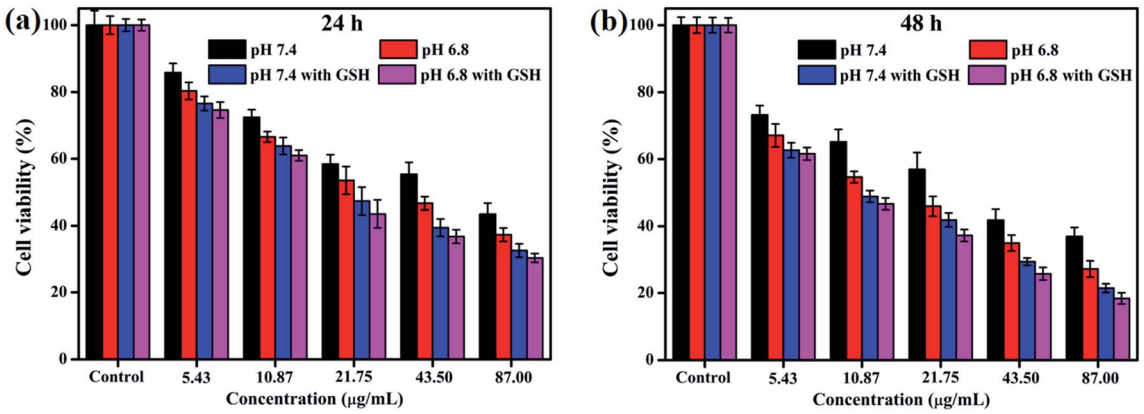

Fig. 3 Cell viability of MGC-803 cells after incubation of CDs–Pt(IV)–PEG for (a) 24 h and (b) 48 h at pH 7.4 or pH 6.8 with or without GSH.

fluorescence imaging behavior of the GES-1 and MGC-803 cells and then quantitatively analyzed by Image-Pro Plus 5.1. When excited at three excitation wavelengths (365, 488, and 543 nm), both the GES-1 and MGC-803 cells fluoresced blue, green and red, respectively, indicating a favorable cellular uptake capability (Fig. 4 and S6†). Specifically, for the MGC-803 cells, the fluorescence intensity at pH 6.8 was stronger than that at pH 7.4, and the ratio of the fluorescence intensity at pH 6.8 to the fluorescence intensity at pH 7.4 was about 1.2. The CDs were still shielded with the PEG polymer at pH 7.4, which resulted in a relatively weaker fluorescence.

The fluorescence intensity of MGC-803 cells was stronger than that of GES-1 cells, and the ratio of the fluorescence intensity of MGC-803 cells to the fluorescence intensity of GES-1 cells was about 1.6 (pH 7.4) or 1.9 (pH 6.8), respectively. As a unique channel for the diffusion of small substances and the regulation and transportation of macromolecules between the nucleus and cytoplasm, nuclear pore complexes (NPCs) provide a way for nanoparticles to enter. There are more NPCs in cancer cells than normal cells, which will provide more possibilities for nanoparticles to enter the cancer nucleus through NPCs.[34] This may be the reason for the high contrast between the fluorescence intensity of GES-1 and MGC-803 cells. In addition, it should be noted that the imaging site of GES-1 and MGC-803 cells also exhibited significant differences. Specifically, the fluorescence was equally dispersed throughout the cancer MGC-803 cells, including the cell nucleus and the cytoplasm. However, the fluorescence was only observed in the cytoplasm in normal gastric cell line GES-1. The results also imply that the system fluorescence model could be used to distinguish between cancer cells and normal cells. The positively charged nanoparticles can escape from lysosome after internalization and exhibit perinuclear localization.[35–37] Nucleus is recognized as one of the most important subcellular targets in nanomedicine, and thus the special properties of the proposed system will contribute to overcome biological barriers and realize effective intracellular drug release.

In order to explore the potential mechanism of the proposed drug delivery system, the zeta potential and particle size were further evaluated under normal physiological condition (pH 7.4) and tumor extracellular microenvironment (pH 6.8). As shown in Fig. 5, the zeta potential and particle size of CDs–Pt(IV)–PEG were neutral and 132.5 d.nm at pH 7.4, and 18.3 mV and 68.06 d.nm at pH 6.8, respectively.

The charge convertibility of CDs–Pt(IV)–PEG was confirmed by zeta potential changes at tumor extracellular pH 6.8 and physiological pH 7.4 (Fig. S7†). Furthermore, at pH 6.8, the zeta potential of CDs–Pt(IV)–PEG showed an increase from −16.6 (negative) to +14.2 (positive) mV with PBS incubation at 37 °C for 4 h. While at pH 7.4 it was not obvious that the zeta potential exhibited charge-convertible phenomenon with PBS incubation at 37 °C for 4 h.

The results indicated that the surface charge and particle size of CDs–Pt(IV)–PEG would be changed to positive and

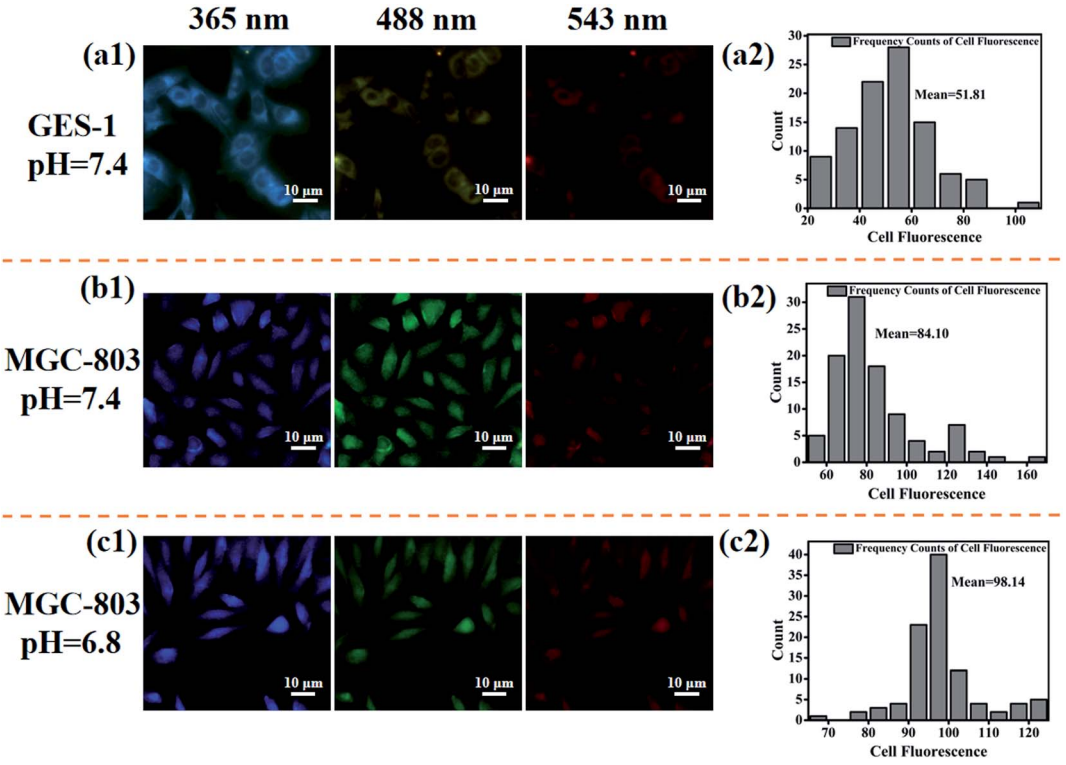

Fig. 4 The fluorescence microscopy images (a1) and the corresponding pixel intensity frequency count (a2) for GES-1 cells at pH 7.4; the fluorescence microscopy images (b1) and the corresponding pixel intensity frequency count (b2) for MGC-803 cells at pH 7.4; the fluorescence microscopy images (c1) and the corresponding pixel intensity frequency count (c2) for MGC-803 cells at pH 6.8.

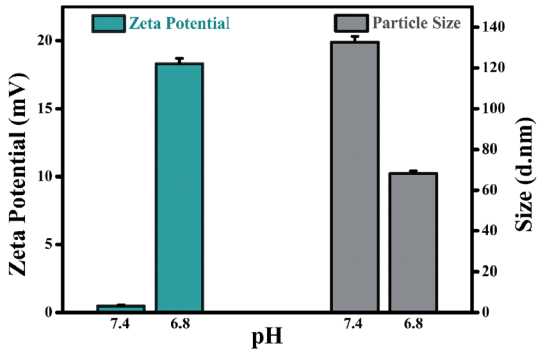

Fig. 5 pH triggered charge/size transitions: zeta potential and particle size.

smaller, respectively. When the CDs–Pt(IV)–PEG reached the tumor site, the weak acidic condition (pH 6.8) could trigger hydrolysis of the benzoic imine bond, resulting in the amines exposure. Subsequently, the zeta potential of the system would rapidly changed from negative to positive. Therefore, the nanocarrier achieved charge conversion and could be easily and effectively internalized by cancer cells with negatively charged cell membranes at acidic pH of tumor microenvironment. Then the loaded cisplatin(IV) prodrug was reduced to cisplatin which showed significant cytotoxicity in reductive cytosol of cancer cells.[5] In the normal microenvironment, the reduction of cisplatin(IV) was very limited, leading to a relatively small toxicity. Thus the pH and redox dual-sensitive characteristics ensure the cancer cells targeting and low side effects on normal cells.

Conclusions

In this study, a nanocarrier drug delivery system (CDs–Pt(IV)–PEG) with the pH and reduction dual-sensitive response characteristics was proposed based on fluorescence CDs. At the weak acidic microenvironment (pH 6.8), the pH-sensitive benzoic imine bond of CDs–Pt(IV)–PEG got hydrolyzed, resulting in the surface charge reversal and size decrease of the drug delivery system. After internalization, under the intracellular reducing microenvironment (ascribed to the intracellular GSH overproduced in tumor cells), the cisplatin(IV) prodrug loaded in CDs–Pt(IV)–PEG was reduced to cisplatin, which resulted in significant cytotoxicity to cancer cells. Additionally, the developed drug delivery system could be able used to distinguish between cancer cells and normal cells by the obvious differences in the imaging site of GES-1 and MGC-803 cells.

Conflicts of interest

The authors declare no conflict of interest.

Acknowledgements

This work was supported by the National Natural Science Foundation of China (Grant No. 51975400, 51622507, 51505324), Basic Research Program of Shanxi for Youths (201701D221111), Scientific and Technological Innovation Programs of Higher Education Institutions in Shanxi (201802036).

References

1 Q. Jia, Z. Zhao, K. Liang, F. Nan, Y. Li, J. Wang, J. Ge and P. Wang, *Mater. Chem. Front.*, 2020, **4**, 449–471.
2 R. L. Siegel, K. D. Miller and A. Jemal, *Ca-Cancer J. Clin.*, 2019, **69**, 7–34.
3 M. Pirsaheb, S. Mohammadi and A. Salimi, *TrAC, Trends Anal. Chem.*, 2019, **115**, 83–99.
4 L. Li, L. Shi, J. Jia, O. Eltayeb and S. Shuang, *ACS Appl. Mater. Interfaces*, 2020, **12**, 18250–18257.
5 T. Feng, X. Ai, H. Ong and Y. Zhao, *ACS Appl. Mater. Interfaces*, 2016, **8**, 18732–18740.
6 T. Feng, X. Ai, G. An, P. Yang and Y. Zhao, *ACS Nano*, 2016, **10**, 4410–4420.
7 D. E. Lee, H. Koo, I. Sun, J. H. Ryu, K. Kim and I. C. Kwon, *Chem. Soc. Rev.*, 2012, **41**, 2656–2672.
8 X. Li, X. Zhang, X. Li and J. Chang, *Cancer Biol. Med.*, 2016, **13**, 339–348.
9 G. Li, M. Pei and P. Liu, *Mater. Sci. Eng., C*, 2020, **110**, 110653.
10 Q. Sun, Z. Zhou, N. Qiu and Y. Shen, *Adv. Mater.*, 2017, **29**, 1606628.
11 K. Ghosal and A. Ghosh, *Mater. Sci. Eng., C: Biomimetic Supramol. Syst.*, 2019, **96**, 887–903.
12 W. Bao, H. Ma, N. Wang and Z. He, *Polym. Adv. Technol.*, 2019, **30**, 2664–2673.
13 V. P. Torchilin, *Nat. Rev. Drug Discovery*, 2014, **13**, 813–827.
14 N. Selvasudha and K. Koumaravelou, *Carbohydr. Polym.*, 2017, **163**, 70–80.
15 S. Fang, J. Lin, C. Li, P. Huang, W. Hou, C. Zhang, J. Liu, S. Huang, Y. Luo and W. Fan, *Small*, 2017, **13**, 1602580.
16 Z. Chen, L. Wan, Y. Yuan, Y. Kuang, X. Xu, T. Liao, J. Liu, Z. Q. Xu, B. Jiang and C. Li, *ACS Biomater. Sci. Eng.*, 2020, **6**, 3375–3387.
17 M. Xue, J. Zhao, Z. Zhan, S. Zhao, C. Lan, F. Ye and H. Liang, *Nanoscale*, 2018, **10**, 18124–18130.
18 C. Wang, Z. Xu and C. Zhang, *ChemNanoMat*, 2015, **1**, 122–127.
19 J. Wang, Y. Zhu and L. Wang, *Chem. Rec.*, 2019, **19**, 2083–2094.
20 Y. Wu, Q. Li, D. Yang and J. Liao, *Nanosci. Nanotechnol. Lett.*, 2017, **9**, 1827–1848.
21 M. Zhang, P. Yuan, N. Zhou, Y. Su, M. Shao and C. Chi, *RSC Adv.*, 2017, **7**, 9347–9356.
22 J. Ma, K. Kang, Y. Zhang, Q. Yi and Z. Gu, *ACS Appl. Mater. Interfaces*, 2018, **10**, 43923–43935.
23 P. Zhang, Y. Wang, J. Lian, Q. Shen, C. Wang, B. Ma, Y. Zhang, T. Xu, J. Li and Y. Shao, *Adv. Mater.*, 2017, **29**, 1702311.
24 Z. Zhang, Y. Lei, X. Yang, N. Shi, L. Geng, S. Wang, J. Zhang and S. Shi, *J. Mater. Chem. B*, 2019, **7**, 2130–2137.
25 S. Niedermayer, V. Weiss, A. Herrmann, A. Schmidt, S. Datz, K. Muller, E. Wagner, T. Bein and C. Brauchle, *Nanoscale*, 2015, **7**, 7953–7964.

26 A. D. Wong, M. Ye, M. B. Ulmschneider and P. C. Searson, *PLoS One*, 2015, **10**, e0123461.
27 J. Chen, J. Ding, Y. Wang, J. Cheng, S. Ji, X. Zhuang and X. Chen, *Adv. Mater.*, 2017, **29**, 1701170.
28 J. Dong, Y. Zhao, H. Chen, L. Liu, W. Zhang, B. Sun, M. Yang, Y. Wang and L. Dong, *New J. Chem.*, 2018, **42**, 14263–14270.
29 H. Wang, J. Di, Y. Sun, J. Fu, Z. Wei, H. Matsui, A. D. C. Alonso and S. Zhou, *Adv. Funct. Mater.*, 2015, **25**, 5537–5547.
30 B. Zhang, G. Zhang, H. Gao, S. Wu, J. Chen and X. Li, *RSC Adv.*, 2015, **5**, 7395–7400.
31 H. Xiao, R. Qi, S. Liu, X. Hu, T. Duan, Y. Zheng, Y. Huang and X. Jing, *Biomaterials*, 2011, **32**, 7732–7739.
32 L. Zhang, Y. Qin, Z. Zhang, F. Fan, C. Huang, L. Lu, H. Wang, X. Jin, H. Zhao, D. Kong, C. Wang, H. Sun, X. Leng and D. Zhu, *Acta Biomater.*, 2018, **15**, 371–385.
33 M. Voigt, I. Bartels, A. Nickisch-Hartfiel and M. Jaeger, *Toxicol. Environ. Chem.*, 2019, **101**, 1–24.
34 T. Jamali, Y. Jamali, M. Mehrbod and M. R. Mofrad, *Int. Rev. Cell Mol. Biol.*, 2011, **287**, 233–286.
35 L. Kou, J. Sun, Y. Zhai and Z. He, *Asian J. Pharm.*, 2013, **8**, 1–10.
36 T. F. Vandamme and L. Brobeck, *J. Controlled Release*, 2005, **102**, 23–38.
37 T. Yeung, G. E. Gilbert, J. Shi, J. R. Silvius, A. Kapus and S. Grinstein, *Science*, 2008, **319**, 210–213.